Thin-Walled Structures 180 (2022) 109947

Contents lists available at ScienceDirect

Thin-Walled Structures

journal homepage: www.elsevier.com/locate/tws

Full length article

Behaviour and design of cold-formed normal- and high-strength steel SHS and RHS columns at elevated temperatures

Han Fang [a,*], Tak-Ming Chan [b,c]

[a] School of Civil Engineering, University of Leeds, United Kingdom[1]
[b] Department of Civil and Environmental Engineering, The Hong Kong Polytechnic University, Hong Kong, China
[c] Chinese National Engineering Research Centre for Steel Construction (Hong Kong Branch), The Hong Kong Polytechnic University, Hong Kong, China

ARTICLE INFO

Keywords:
Cold-formed SHS and RHS columns
Normal- and high-strength steel
Finite element modelling
Elevated temperatures
Design

ABSTRACT

The behaviour of cold-formed normal- and high-strength steel columns with square and rectangular hollow sections (SHSs and RHSs) at elevated temperatures was investigated numerically in this paper. A finite element model was developed and validated against experimental results for the cold-formed steel SHS and RHS stub and long columns tested at ambient and elevated temperatures. Parametric studies were subsequently conduced on cold-formed normal- and high-strength steel SHS and RHS columns with various cross-section slenderness and member slenderness at elevated temperatures ranging from ambient to 800 °C. Based on the numerical results and experimental results reported in literature, the applicability of existing design approaches in European and North American standards to the columns at elevated temperatures was evaluated. The evaluation shows that the approaches in standards provide quite conservative strength predictions for the cold-formed normal- and high-strength steel SHS and RHS columns at elevated temperatures except for the overestimation of cross-sectional resistance obtained based on the North American standard. Modified design approaches were proposed to improve the accuracy of strength predictions and can be safely applied to generate designs for the columns under various elevated temperatures.

1. Introduction

Cold-formed steel hollow section structures have been widely applied in the construction industry for buildings, bridges and offshore platforms, owing to their high resistance to buckling and aesthetic appearance [1–3]. In addition to the widely used normal-strength steel for fabricating these structures, high-strength steel with nominal yield strength above 460 MPa has gained increasing popularity in the construction industry and can be used to form the cold-formed hollow section structures with higher strength, reduced sizes and lower embodied carbon footprint [4–7]. In order to implement the structures formed with high-strength steel, extensive research studies have been conducted to investigate the behaviour and design of cold-formed high-strength steel hollow section structures subject to compression [3,8–10], bending [11] or combined compression and bending [12–14]. These research studies primarily focused on the structural performance under the ambient temperature condition. However, structures can be subject to elevated temperatures due to the occurrence of fire which causes significant damages to steel structures since the strength and stiffness of the material deteriorate with increasing temperatures [15–18]. Therefore, the behaviour of the structures at elevated temperatures needs to be fully understood in order to conduct fire resistance design.

Previous studies with the consideration of elevated temperature conditions mainly focused on the hot-finished hollow section structures [22–24]. Compared with the hot-finished structures, the structures fabricated through cold-forming processes can have different material properties, residual stresses and geometric imperfections which all can influence the structural performance [19,25]. Limited research studies were performed on the cold-formed hollow section structures at elevated temperatures and are reviewed here. Feng et al. [26] performed numerical simulations on cold-formed SHS columns made of the S355 grade steel at two elevated temperatures of 400 °C and 600 °C. In the study, it was found that the resistance of the columns at elevated temperatures was dependent on the global geometric imperfection magnitudes. They also compared the ultimate loads of the columns from numerical simulations with those predicted based on European standard [27] and found that conservative strength predictions were obtained. Balarupan and Mahendran [21] conducted experiments on nine cold-formed SHS columns at ambient and elevated temperatures up to 700 °C. The columns with two cross-sectional sizes and the same length were fabricated using the steel with nominal yield strength of 450 MPa. Through the experimental investigations, the columns were found to experience significant strength decrement with increasing temperatures. The ultimate loads for the columns from experiments were

* Corresponding author.
E-mail address: H.Fang1@leeds.ac.uk (H. Fang).
[1] Formerly, School of Civil, Environmental and Mining Engineering, The University of Adelaide, South Australia 5005, Australia.

https://doi.org/10.1016/j.tws.2022.109947
Received 11 April 2022; Received in revised form 27 June 2022; Accepted 29 July 2022
Available online 22 August 2022

Table 1
Dimensions and parameters of cold-formed SHS and RHS columns tested at ambient and elevated temperatures.

Specimen	B (mm)	H (mm)	t (mm)	Steel grade	Boundary conditions	L (mm)	Temperature conditions
H80 × 80 × 4-S [10]	80.4	80.1	3.94	S700	Fixed	240	Ambient
H100 × 100 × 4-S [10]	100.5	100.2	3.92	S700	Fixed	300	Ambient
H120 × 120 × 4-S [10]	120.9	120.7	3.92	S700	Fixed	360	Ambient
H140 × 140 × 5-S [10]	140.2	141.0	4.94	S700	Fixed	420	Ambient
H140 × 140 × 6-S [10]	141.1	141.1	5.96	S700	Fixed	420	Ambient
H160 × 160 × 4-S [10]	160.5	160.3	3.97	S700	Fixed	480	Ambient
H100 × 50 × 4-S [10]	100.2	50.5	3.94	S700	Fixed	300	Ambient
H200 × 120 × 5-S [10]	200.3	120.5	4.94	S700	Fixed	565	Ambient
V80 × 80 × 4-S [10]	80.4	80.2	3.94	S900	Fixed	240	Ambient
V100 × 100 × 4-S [10]	100.3	100.4	3.97	S900	Fixed	300	Ambient
V120 × 120 × 4-S [10]	121.2	121.4	3.92	S900	Fixed	360	Ambient
SHS 100 × 100 × 4-CF1 [19]	100.6	100.5	3.59	S355	Fixed	405	Ambient
SHS 60 × 60 × 3-CF1 [19]	60.1	60.3	2.78	S355	Fixed	245	Ambient
H80 × 80 × 4-LBC [20]	80.3	80.1	3.94	S700	Pinned	1480	Ambient
H100 × 50 × 4-LBC [20]	100.2	50.6	3.97	S700	Pinned	1480	Ambient
H50 × 100 × 4-LBC [20]	50.3	100.2	3.98	S700	Pinned	1480	Ambient
65 × 65 × 3-room [21]	65.0	65.0	3.00	G450	Fixed	1800	Ambient
65 × 65 × 3-T200 [21]	65.0	65.0	3.00	G450	Fixed	1800	200 °C
65 × 65 × 3-T400 [21]	65.0	65.0	3.00	G450	Fixed	1800	400 °C
65 × 65 × 3-T500 [21]	65.0	65.0	3.00	G450	Fixed	1800	500 °C
65 × 65 × 3-T600 [21]	65.0	65.0	3.00	G450	Fixed	1800	600 °C
65 × 65 × 3-T700 [21]	65.0	65.0	3.00	G450	Fixed	1800	700 °C
65 × 65 × 6-T500 [21]	65.0	65.0	6.00	G450	Fixed	1800	500 °C
65 × 65 × 6-T600 [21]	65.0	65.0	6.00	G450	Fixed	1800	600 °C
65 × 65 × 6-T700 [21]	65.0	65.0	6.00	G450	Fixed	1800	700 °C

also compared with the strength predictions based on European [27] and North American [28] standards. The comparison showed that the European and North American standards primarily provide conservative strength predictions. From these existing research studies, it is evident that these investigations focused on structures with a specific steel grade and limited range of dimensions. Besides, the behaviour of the cold-formed SHS and RHS columns formed using steel with higher grades and subject to elevated temperatures remains unexplored.

Therefore, in this study, the behaviour of cold-formed normal- and high-strength steel SHS and RHS columns at elevated temperatures was investigated numerically. A finite element model was developed and validated using the experimental results reported in literature for cold-formed normal- and high-strength steel SHS and RHS columns tested under ambient and elevated temperatures. Parametric studies were subsequently performed on cold-formed SHS and RHS columns with various cross-sectional dimensions, member slenderness and steel grades and subject to elevated temperatures ranging from 20 to 800 °C. Furthermore, the applicability of design specifications in Eurocode 3 and AISC 360 standards to the structures at various elevated temperatures was evaluated based on the results of parametric studies in this study and experimental results in literature. Based on the evaluation, design approach modifications were also proposed.

2. Numerical modelling

Numerical investigations on cold-formed normal- and high-strength steel SHS and RHS columns at elevated temperatures were performed through finite element (FE) modelling using the software package ABAQUS 6.14 [29]. Compared with physical testing of the structures, the finite element modelling methodology is economical and efficient for the investigations on structures at elevated temperatures [30–32]. A FE model was developed and validated using the experimental results for the cold-formed normal- and high-strength steel SHS and RHS stub and long columns at ambient and elevated temperatures [10,19–21], as shown in Table 1 for the summary of experimental results in literature based on the nomenclature defined in Fig. 1.

2.1. Finite element model

The cold-formed normal- and high-strength steel SHS and RHS stub and long columns were simulated using the four-noded shell

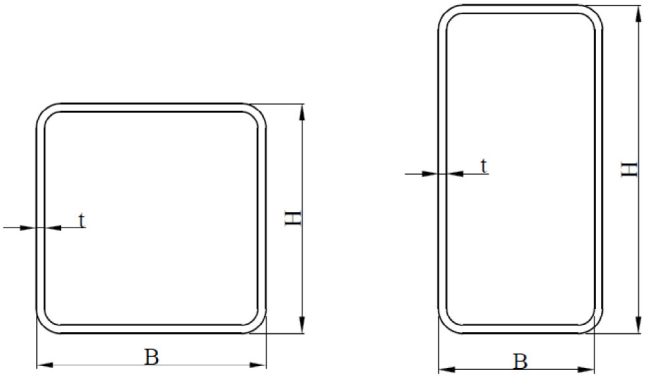

Fig. 1. Symbols of the SHS and RHS.

elements S4R with reduced integration [33–35]. The element mesh size of about the same as the plate thickness of the columns was adopted through mesh sensitivity analysis. To accurately simulate the structural behaviour, the material properties for the columns provided in the experimental investigations [10,20,21,36] were employed. As for the cold-formed stub columns tested by Gardner et al. [19] at the ambient temperature, the stress–strain relationship was obtained using the model provided by Gardner and Yun [37] for cold-formed steel hollow sections since no completed material stress–strain relationship was provided. The stress–strain relationship obtained at ambient and elevated temperatures for the respective columns were converted into the true stress versus log plastic strain relationship which was subsequently substituted as the input for the modelling.

Initial local and global geometric imperfections can influence the behaviour of the cold-formed normal- and high-strength steel hollow section columns [4,8,38]. To take this effect into account, the lowest local and global eigenmode shapes for the columns obtained through separate linear eigenvalue buckling analysis were used as the geometric imperfection shapes. For the stub columns tested in Ma et al. [10] and Gardner et al. [19], the obtained geometric imperfection shapes were scaled with the local geometric imperfection magnitudes measured in those studies for model validation and no global geometric imperfections were considered since the governing failure mode is local buckling. For the long columns tested at ambient

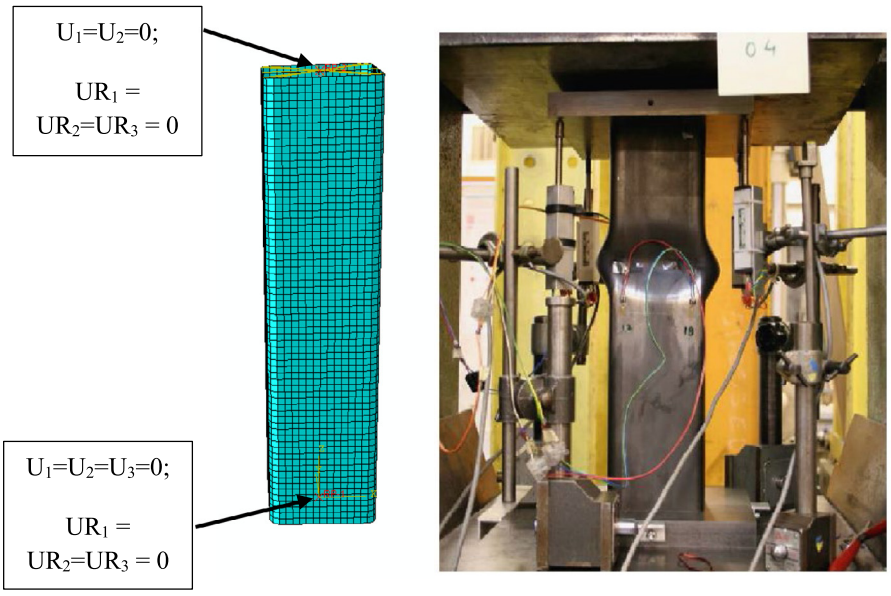

(a) Stub column based on the experiment in [19].

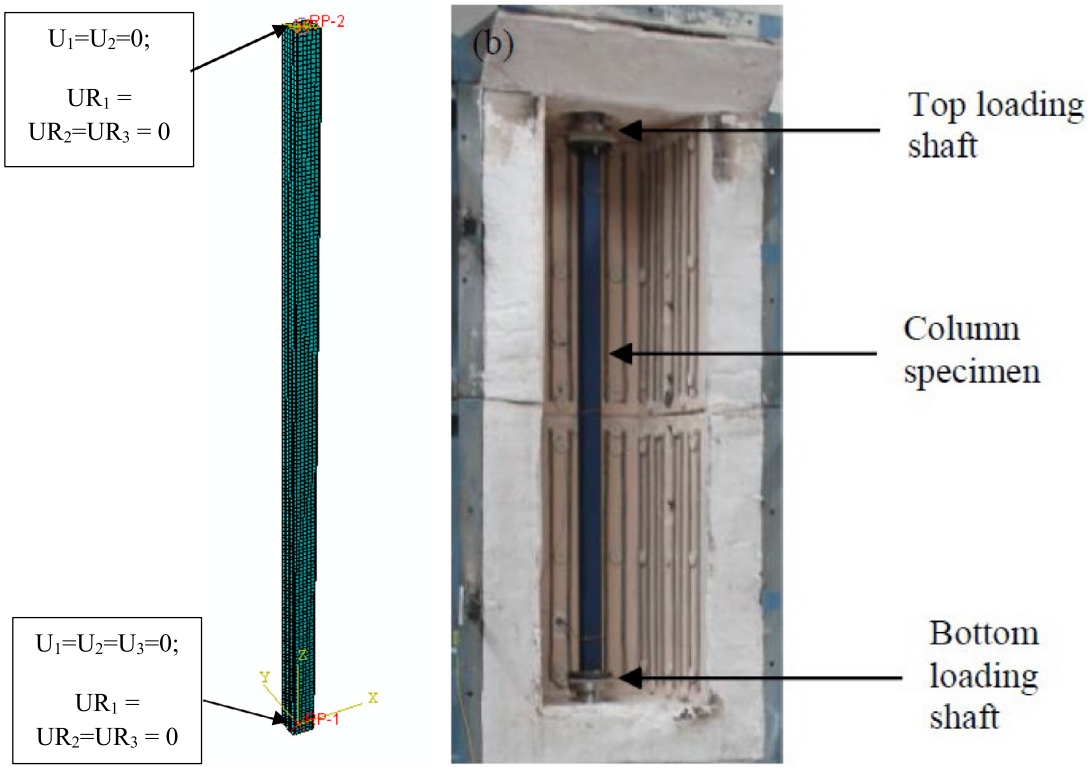

(b) Long column based on the experiment reported in [21].

Fig. 2. Typical FE models compared with experimental conditions.

and elevated temperatures, the measured magnitudes of the local and global imperfections [10,20,21] were adopted for the FE modelling of the structures. Since no local geometric imperfections were provided for the columns tested by Balarupan and Mahendran [21], the imperfection magnitudes provided by Gardner et al. [19] for cold-formed SHS were adopted.

Apart from the geometric imperfections, membrane and bending residual stresses were found to exist in the cold-formed hollow sections due to the fabrication processes. The bending residual stresses were inherently incorporated by applying the input material properties measured for specimens extracted from the cold-formed hollow sections [8,14,39]. The effect of bending residual stresses was introduced in the

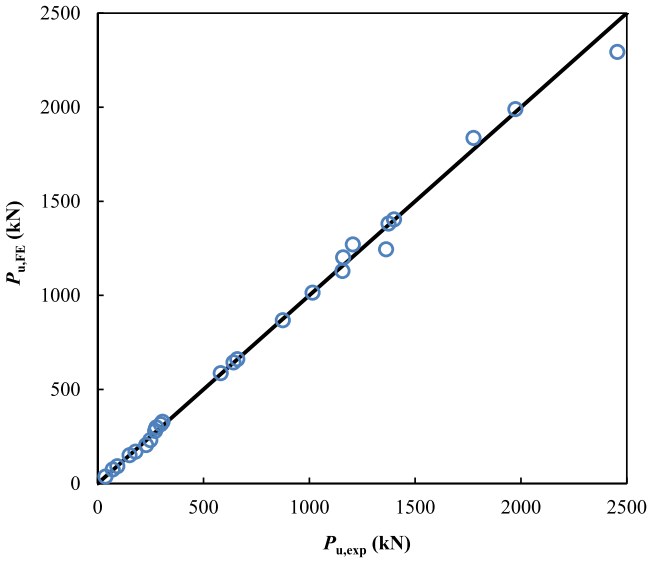

Fig. 3. Comparison of the obtained $P_{u,FE}$ for cold-formed SHS and RHS stub columns with different steel grades with the $P_{u,exp}$ from experiments [10,19–21].

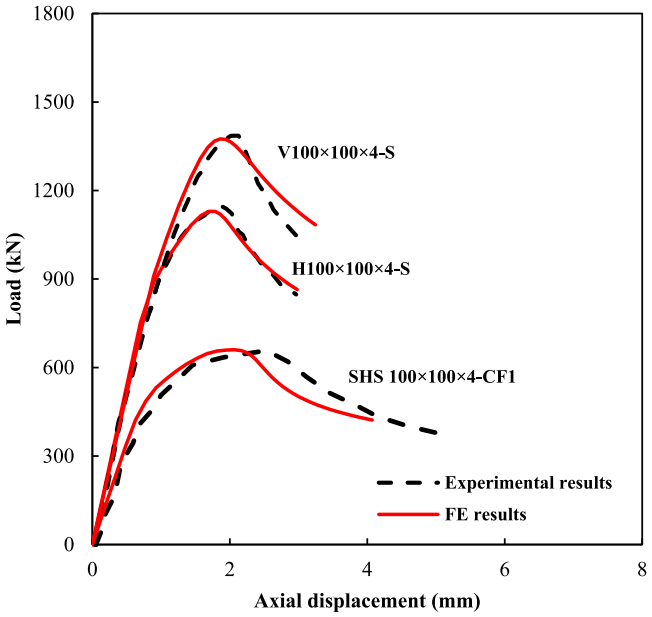

Fig. 4. Comparison of the load versus axial displacement responses predicted in FE modelling with experimental results reported in literature for typical stub columns [10,19].

material properties measurement tests by straightening the specimens with curved shapes due to the release of bending residual stresses in the process of extracting the specimens from the cold-formed hollow sections [39,40]. As for the membrane residual stresses, their effect on the behaviour of columns was found to be quite limited [8,14]. Thus, membrane residual stresses were not taken into account in the FE model.

The boundary conditions used in the experiments for the columns were also simulated in the model using reference points coupled with the nodes of end surfaces of each column. For the columns tested under fixed-ended conditions, all degrees of freedom at the reference points were restrained except for the longitudinal translation. For the pin-ended columns, the rotations about the buckling axis at two ends and the displacement in the direction of loading at the loaded end were allowed at the respective reference points while other degrees

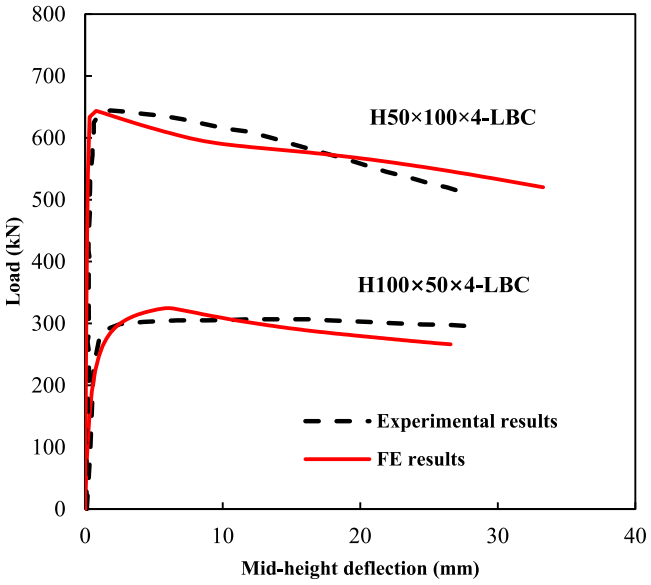

Fig. 5. Comparison of the load versus mid-height deflection responses predicted in FE modelling with experimental results reported in literature [20] for typical long columns.

of freedoms were restrained. Typical FE models for stub and long columns are shown in Fig. 2 in comparison with the column specimens in experimental investigations. The load was subsequently applied through the reference point on the loaded side by specifying an axial displacement in a static RIKS step employed to predict the behaviour of the structures.

2.2. Validation

The FE model described in the previous section was validated by comparing the FE results with the experimental results reported in literature for cold-formed normal- or high-strength steel SHS and RHS stub and long columns tested at ambient and elevated temperatures [10,19–21]. The ultimate loads ($P_{u,FE}$) from FE modelling were firstly compared with those ($P_{u,exp}$) obtained in experiments, as shown in Fig. 3. As can be seen in the figure, the ultimate loads were accurately predicted, with the mean $P_{u,FE}/P_{u,exp}$ ratio of 1.00 and the coefficient of variation (CoV) of 0.04.

The load–displacement responses predicted in FE modelling were also compared with the experimental results. The comparison of the load versus axial displacement responses from FE modelling and experiments for typical stub columns is presented in Fig. 4 while the comparison of load versus mid-height deflection for typical long columns is provided in Fig. 5. It can be observed in these figures that the load–displacement responses for cold-formed SHS and RHS stub and long columns were replicated by the FE model. Furthermore, the predicted local or global buckling failure modes of the structures also compared well with the failure mode observations from experimental investigations, as shown in Fig. 6 for typical stub and long columns. These comparisons between the results from FE modelling and experimental investigations demonstrate that the FE model can provide accurate predictions of the behaviour of cold-formed normal- and high-strength steel SHS and RHS stub and long columns at ambient and elevated temperatures.

3. Parametric study

With the validated FE model, systematic parametric studies were performed on cold-formed normal- and high-strength steel SHS and RHS stub and long columns at elevated temperatures ranging from

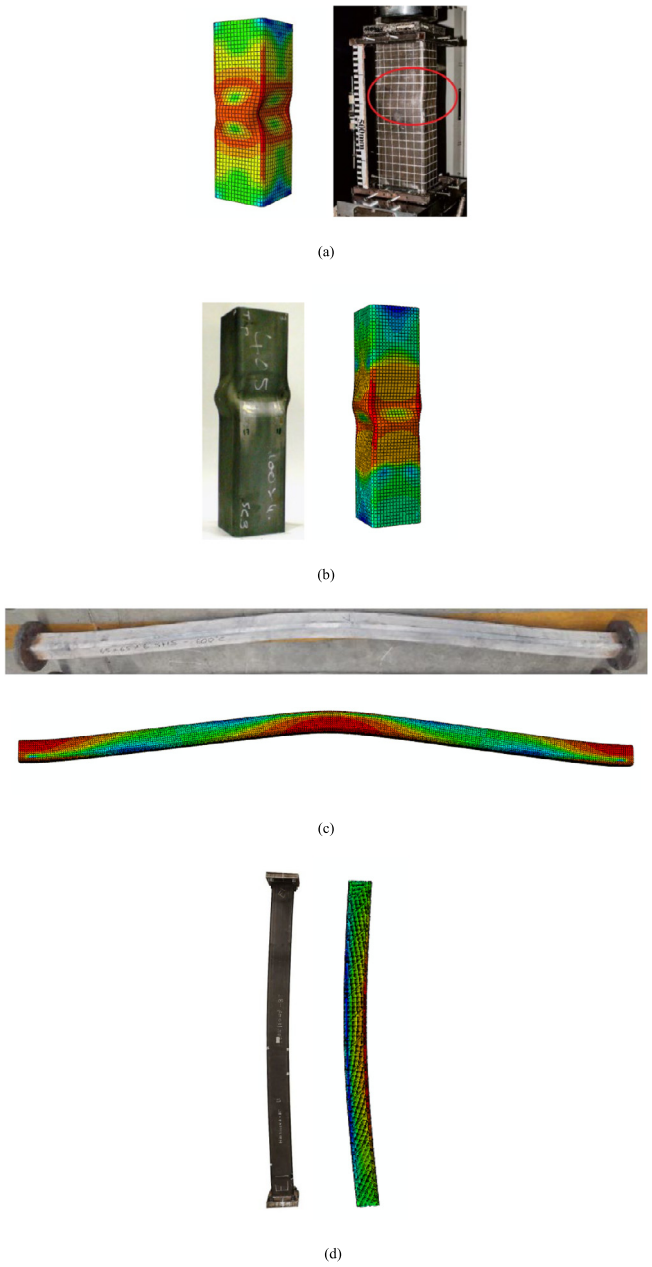

Fig. 6. Comparison of the failure modes predicted in FE modelling with the experimental observations for (a) H160 × 160 × 4-S [10]; (b) SHS 100 × 100 × 4-CF1 [19]; (c) 65 × 65 × 6-T600 [21] and (d) H50 × 100 × 4-LBC [20].

ambient temperature to 800 °C (ambient temperature, 200 °C, 400 °C, 600 °C and 800 °C). A variety of parameters for the cross-sectional dimensions, member slenderness ratios and steel grades were considered. For the SHS columns, the dimension for B and H of the cross-sections equals to 140 mm while varying plate thicknesses between 3 mm and 7 mm were used to obtain the Class 1–3 and Class 4 cross-sections according to the European standard [27]. For the RHS columns, the width B and height H as 100 mm and 200 mm respectively were used while the plate thickness varied between 4 mm and 10 mm to obtain Class 1–4 cross-sections. The length for the fixed-ended stub columns was taken as three times of the H of the cross-sections to avoid the occurrence of global buckling [10,19]. For the pin-ended long columns, member slenderness as the effective length over radius of gyration ratio (L/r) is ranged from about 20 to 100 by adopting different effective lengths for the columns. For RHS long columns, the buckling about both major and minor axes was considered.

For these stub and long columns, grades of S355, S450, S700 and S900 to cover normal- and high-strength steel were considered. The material properties, especially the stress–strain relationship, for these grades of steel in cold-formed sections at the ambient temperature, were obtained based on the models proposed in previous studies [36,37,41]. As for the elevated temperature conditions, the material properties such as the elastic modulus, yield strength, and ultimate strength were obtained based on the nominal values at the ambient temperature and reduction factors for the properties of those steel grades based on experimental investigations [18,36,42]. The stress–strain relationship at the elevated temperatures was generated based on the model in Imran et al. [42] for S355 steel, the model in [36] for S450 steel and that in Li et al. [43] for S700 and S900 high-strength steel. Apart from the input of material properties, initial geometric imperfections were also incorporated. For the magnitudes of local geometric imperfections, the magnitudes suggested by Gardner et al. [19] for cold-formed normal-strength steel SHS and RHS was adopted while the magnitudes given by Ma et al. [10] for those sections fabricated with S700 and S900 high-strength steel were used. For the global geometric imperfections, the magnitude as effective length over 1000 was found to be suitable for cold-formed SHS and RHS long columns [44] and was used in the parametric study.

4. Design approaches

With the numerical results generated in this study and the experimental results in literature, the applicability of design approaches in Eurocode 3 and AISC 360 standards to the cold-formed normal- and high-strength steel SHS and RHS columns was assessed. The strength predictions for SHS and RHS stub and long columns investigated in parametric studies were obtained based on the material properties used for the modelling. As for the structures from experimental investigations in literature, the material properties in those studies were used for estimating the ultimate loads. The predicted ultimate loads (P_u) were compared with the $P_{u,FE+exp}$ from parametric studies and experimental results. The accuracy of the approaches for strength predictions is discussed in the subsequent sections. Modifications to the design approaches were also proposed to generate more accurate predictions.

4.1. Evaluation of existing design approaches

4.1.1. Eurocode 3

The Eurocode 3 provides design approaches in the Part 1–2 [27] for steel stub and long columns at elevated temperatures. For the SHS and RHS stub columns subject to axial compression, the resistance of the structures with Class 1–3 (non-slender) or Class 4 (slender) cross-sections can be estimated using Eq. (1). In the equation, A and A_{eff} are the gross and effective cross-sectional area respectively, $f_{2,\theta}$ is the stress corresponding to 2% strain at elevated temperatures and $f_{0.2,\theta}$ is the 0.2% proof strength of the material at elevated temperatures. The A_{eff} for Class 4 cross-sections can be estimated based on the effective width (b_e) calculated using Eq. (2) provided in the Part 1–5 of Eurocode 3 [45,46]. In Eq. (2), b is the plate width excluding the corner regions, $\overline{\lambda}_p$ is the non-dimensional slenderness of a plate element in any SHS or RHS and ψ is the stress ratio based on the stress distribution. The determination of cross-section classification is based on the parameter ε_θ which is defined in Eq. (3). In Eq. (3), the value 0.85 is given in the standard as the averaged value of the square root for the ratios of reduction factor for elastic modulus ($k_{E,\theta}$) over that for yield strength ($k_{y,\theta}$) at elevated temperatures. As for the long columns, the resistance can be estimated by multiplying the cross-section resistance calculated from Eq. (1) by the reduction factor (χ_{EC}) for flexural buckling. The χ_{EC} is estimated using Eqs. (4)–(7). In the equations, $\overline{\lambda}$ is the non-dimensional member slenderness at the ambient temperature and can be estimated from Eq. (8) where N_{cr} is the elastic critical force.

$$P_{EC3} = \begin{cases} A \times f_{2,\theta} \ for\ Class\ 1-3\ cross-sections \\ A_{eff} \times f_{0.2,\theta} \ for\ Class\ 4\ cross-sections \end{cases} \quad (1)$$

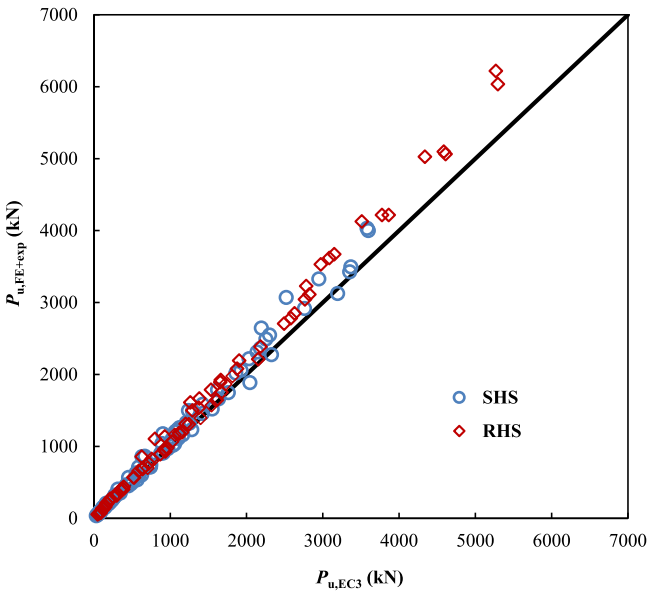

Fig. 7. Comparison of the strength predictions based on Eurocode 3 for cold-formed SHS and RHS stub columns with those from parametric studies and experimental results in literature [10,19].

$$b_e = \mathrm{b} \times \frac{\overline{\lambda_p} - 0.055\,(3+\psi)}{\overline{\lambda_p}^2} \quad for\ \overline{\lambda_p} > 0.5 + \sqrt{0.085 - 0.055\psi} \tag{2}$$

$$\varepsilon_\theta = 0.85 \times \sqrt{\frac{235}{f_y}} \tag{3}$$

$$\chi_{EC} = \frac{1}{\varphi_\theta + \sqrt{\varphi_\theta^2 - \overline{\lambda_\theta}^2}} \tag{4}$$

$$\varphi_\theta = \frac{1}{2}\left[1 + \alpha\overline{\lambda_\theta} + \overline{\lambda_\theta}^2\right] \tag{5}$$

$$\alpha = 0.65 \times \sqrt{235/f_y} \tag{6}$$

$$\overline{\lambda_\theta} = \overline{\lambda}\left[k_{y,\theta}/k_{E,\theta}\right]^{0.5} \tag{7}$$

$$\overline{\lambda} = \begin{cases} \sqrt{\dfrac{A \times f_y}{N_{cr}}} & for\ Class\ 1-3\ cross-sections \\ \sqrt{\dfrac{A_{eff} \times f_y}{N_{cr}}} & for\ Class\ 4\ cross-sections \end{cases} \tag{8}$$

The strengths ($P_{u,EC3}$) estimated based on these equations are compared with the $P_{u,FE+exp}$ for the cold-formed SHS and RHS stub and long columns made of normal- and high-strength steel, as shown in Figs. 7 and 8 for stub and long columns respectively. As can be seen in the figures, the ultimate loads for the columns were underestimated. For the stub columns with SHS and RHS, the mean $P_{u,FE+exp}/P_{u,EC3}$ ratios are about 1.03–1.16 with the CoV as 0.02–0.10, as shown in Tables 2 and 3 respectively. As for the long columns, the mean $P_{u,FE+exp}/P_{u,EC3}$ ratios are about 1.20–1.40 with CoV of 0.09–0.18, as shown in Table 4.

4.1.2. AISC 360

AISC 360 provides the specifications for steel structural design at elevated temperatures in Appendix 4. The resistance of columns can be estimated from Eq. (9) using the material properties at elevated temperatures. The $F_{cr,\theta}$ is the critical stress at elevated temperatures and can be calculated using Eq. (10) given for the elevated temperature conditions. In Eq. (10), $F_{e,\theta}$ is the elastic buckling stress at elevated temperatures. For the stub and long columns with slender cross-sections, the estimation of b_e for the slender plate elements in the cross-sections is specified in the standard for determining A_{eff}, as given in Eq. (11). The $F_{el,\theta}$ is the elastic local buckling stress at

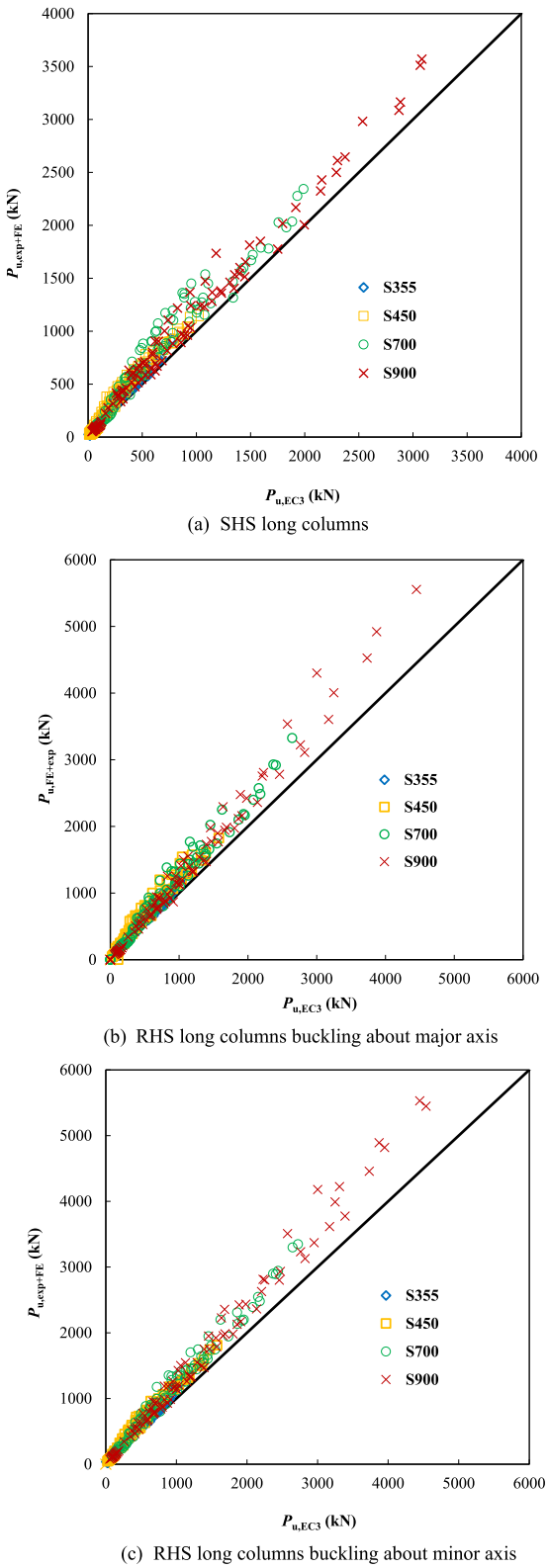

Fig. 8. Comparison of the strength predictions based on Eurocode 3 for cold-formed SHS and RHS long columns with those from parametric studies and experimental results in literature [20,21].

elevated temperatures and estimated based on Eq. (12) where λ is the width-to-thickness ratio for the plate element and λ_r is the limiting width-to-thickness ratio as given in Eq. (13) where E_θ is the elastic modulus at elevated temperatures. While calculating the $P_{u,AISC}$ for

Table 2
Statistic evaluation of strength predictions based on design approaches for cold-formed SHS stub columns at ambient and elevated temperatures.

Steel grade	Cross-section classification	Parameters	$P_{u,FE+Exp}/P_{u,EC3}$	$P_{u,FE+Exp}/P_{u,AISC}$	$P_{u,FE+Exp}/P_{u,modEC3}$	$P_{u,FE+Exp}/P_{u,modAISC}$
S355	Non-slender	Mean	1.03	1.01	–	–
		COV	0.03	0.04	–	–
	Slender	Mean	1.04	0.91	1.04	1.05
		COV	0.04	0.04	0.04	0.05
S450	Non-slender	Mean	1.04	0.02	–	–
		COV	0.10	0.10	–	–
	Slender	Mean	1.04	0.87	1.04	1.06
		COV	0.06	0.03	0.02	0.06
S700	Non-slender	Mean	1.10	1.09	–	–
		COV	0.02	0.02	–	–
	Slender	Mean	1.15	0.99	1.03	1.02
		COV	0.10	0.08	0.07	0.06
S900	Non-slender	Mean	1.09	1.09	–	–
		COV	0.04	0.04	–	–
	Slender	Mean	1.13	0.98	1.05	1.04
		COV	0.10	0.08	0.06	0.06

Table 3
Statistic evaluation of strength predictions based on design approaches for cold-formed RHS stub columns at ambient and elevated temperatures.

Steel grade	Cross-section classification	Parameters	$P_{u,FE+Exp}/P_{u,EC3}$	$P_{u,FE+Exp}/P_{u,AISC}$	$P_{u,FE+Exp}/P_{u,modEC3}$	$P_{u,FE+Exp}/P_{u,modAISC}$
S355	Non-slender	Mean	1.06	1.06	–	–
		COV	0.03	0.03	–	–
	Slender	Mean	1.07	0.95	1.01	1.01
		COV	0.05	0.02	0.05	0.06
S450	Non-slender	Mean	1.05	1.05	–	–
		COV	0.04	0.04	–	–
	Slender	Mean	1.09	0.95	1.01	1.01
		COV	0.05	0.02	0.04	0.03
S700	Non-slender	Mean	1.13	1.13	–	–
		COV	0.03	0.03	–	–
	Slender	Mean	1.16	1.12	1.01	1.03
		COV	0.10	0.10	0.03	0.02
S900	Non-slender	Mean	1.15	1.15	–	–
		COV	0.03	0.03	–	–
	Slender	Mean	1.16	1.07	1.04	1.05
		COV	0.06	0.07	0.04	0.05

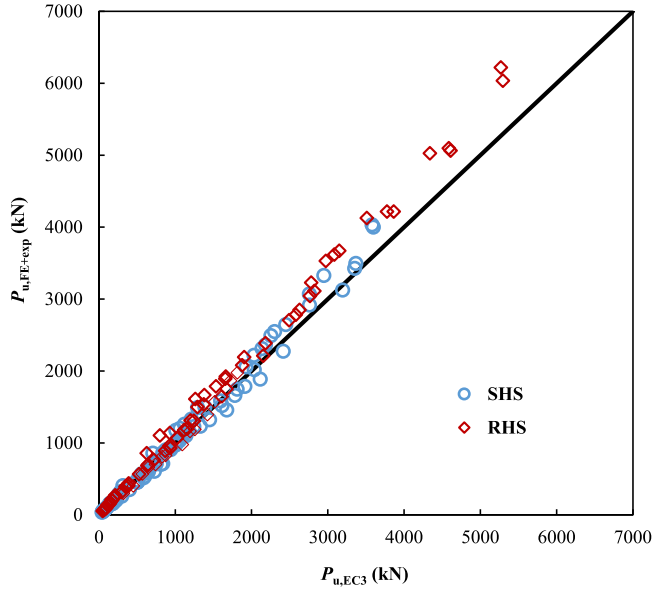

Fig. 9. Comparison of the strength predictions based on AISC 360 for cold-formed SHS and RHS stub columns with those from parametric studies and experimental results in literature [10,19].

stub columns, the $F_{cr,\theta}$ in Eqs. (9) and (11) can be taken as the yield strength at elevated temperatures ($f_{y,\theta}$) [47]. In order to have the direct comparison with the design specifications from Eurocode 3, the $f_{y,\theta}$ for strength predictions followed the same arrangements as that based on Eurocode 3, as presented in Eq. (1).

$$P_{AISC} = \begin{cases} A \times F_{cr,\theta} \ for\ non-slender\ cross-sections \\ A_{eff} \times F_{cr,\theta} \ for\ slender\ cross-sections \end{cases} \quad (9)$$

$$F_{cr,\theta} = \left[0.42^{\sqrt{\frac{f_{y,\theta}}{f_{e,\theta}}}}\right] \times f_{y,\theta} \quad (10)$$

$$b_e = b \times \left(1 - 0.2 \times \sqrt{\frac{F_{el,\theta}}{F_{cr,\theta}}}\right) \sqrt{\frac{F_{el,\theta}}{F_{cr,\theta}}} \quad (11)$$

$$F_{el,\theta} = \left(1.38 \times \frac{\lambda_r}{\lambda}\right)^2 \times f_{y,\theta} \quad (12)$$

$$\lambda_r = 1.4 \times \sqrt{\frac{E_\theta}{f_{y,\theta}}} \quad (13)$$

The strength predictions based on AISC 360 are compared with those from the numerical results in this study and experimental results in literature, as shown in Figs. 9 and 10 for stub and long columns respectively. The statistical evaluation for the accuracy of strength predictions is provided in Tables 2–4. As can be observed in Fig. 9 and Tables 2 and 3, overestimations of the ultimate loads by 1%–13% on average were obtained mainly for the SHS and S355 and S450

Table 4
Statistic evaluation of strength predictions based on design approaches for cold-formed SHS and RHS long columns at ambient and elevated temperatures.

Cross-section shape	Steel grade	Buckling axis	Parameters	$P_{u,FE+Exp}/P_{u,EC3}$	$P_{u,FE+Exp}/P_{u,AISC}$	$P_{u,FE+Exp}/P_{u,modEC3}$	$P_{u,FE+Exp}/P_{u,modAISC}$
SHS	S355	–	Mean	1.31	1.39	1.20	1.25
			COV	0.11	0.09	0.10	0.10
	S450	–	Mean	1.40	1.46	1.33	1.26
		–	COV	0.12	0.11	0.14	0.12
	S700	–	Mean	1.33	1.50	1.17	1.29
			COV	0.16	0.12	0.12	0.16
	S900	–	Mean	1.22	1.42	1.10	1.24
			COV	0.13	0.10	0.12	0.13
RHS	S355	Major axis	Mean	1.27	1.38	1.15	1.18
			COV	0.10	0.08	0.08	0.06
		Minor axis	Mean	1.26	1.36	1.14	1.18
			COV	0.10	0.08	0.08	0.08
	S450	Major axis	Mean	1.36	1.40	1.16	1.20
			COV	0.18	0.15	0.11	0.09
		Minor axis	Mean	1.32	1.41	1.18	1.21
			COV	0.12	0.14	0.10	0.08
	S700	Major axis	Mean	1.27	1.45	1.14	1.23
			COV	0.12	0.11	0.10	0.11
		Minor axis	Mean	1.26	1.45	1.13	1.23
			COV	0.10	0.08	0.07	0.08
	S900	Major axis	Mean	1.20	1.43	1.09	1.20
			COV	0.09	0.09	0.08	0.10
		Minor axis	Mean	1.21	1.47	1.10	1.20
			COV	0.09	0.11	0.07	0.09

RHS stub columns with slender sections while underestimations by 1%–13% on average were generated for the stub columns with non-slender sections and different steel grades. As for the long columns, the strength predictions are quite conservative with the mean $P_{u,FE+exp}/P_{u,AISC}$ ratios of about 1.36–1.50 and the CoV of 0.08–0.15, as shown in Table 4.

4.2. Modified design approaches

4.2.1. Design approaches for resistance of stub columns with slender cross-sections

The evaluation of design approaches for estimating the resistance of stub columns demonstrates that the AISC 360 can provide unconservative strength predictions for the structures with slender cross-sections while underestimations up to 16% on average were obtained based on Eurocode 3. These results indicate that more accurate design approaches are required for estimating the resistance of the stub columns with slender cross-sections. The modifications to the specifications based on effective width methods in Eurocode 3 and AISC 360 are described separately in the subsequent sections.

4.2.1.1. Modification to Eurocode 3. To improve the accuracy of strength predictions for each SHS or RHS stub column with a slender cross-section, the strength contribution ($P_{u,plate}$) from the plate element undergoing local buckling to the ultimate capacity of each stub column was obtained from the FE modelling. The $P_{u,plate}$ values normalised by $A \times f_{0.2,\theta}$ are plotted against $\overline{\lambda_p}$ estimated according to Eurocode 3, as shown in Fig. 11(a). From the figure, it can be observed that the $P_{u,plate}$ can be higher than $A \times f_{0.2,\theta}$, revealing that using $f_{0.2,\theta}$ can lead to quite conservative strength predictions. Besides, the high scattering and conservative predictions may be also due to the lack of accurate consideration for the reduced elastic modulus and yield strength at different elevated temperatures which can influence the resistance of stub columns that undergo local buckling [30]. According to Eurocode 3, the 0.85 in Eq. (3) refers to the averaged value of the square root for the $k_{E,\theta}$ over $k_{y,\theta}$ ratios ($[k_{E,\theta}/k_{y,\theta}]^{0.5}$). However, the $[k_{E,\theta}/k_{y,\theta}]^{0.5}$ varies between about 0.91 and 1.97 for steel in different grades according to the measurements of material properties at elevated temperatures [18,36,42].

In order to generate more accurate and consistent predictions, the $\varepsilon_{\theta,mod}$ can be estimated using Eq. (14) based on the measured $k_{E,\theta}$ and $k_{y,\theta}$ for steel in different grades and used for estimating $\overline{\lambda}_{p,mod}$ to accurately incorporate the variation of elastic modulus and yield strength with different temperatures. The $f_{2,\theta}$ was employed for the strength predictions to be consistent with that applied to the non-slender cross-sections and to reduce the conservatism of strength predictions for the stub columns with Class-4 sections and relatively lower plate slenderness. To develop a suitable approach for strength predictions, the $P_{u,plate}$ values normalised by $A \times f_{2,\theta}$ are plotted against $\overline{\lambda}_{p,mod}$ obtained using $\varepsilon_{\theta,mod}$ calculated from Eq. (14), as presented in Fig. 11(b). As can be seen in the figure, the $P_{u,plate}/A \times f_{2,\theta}$ decreases with increasing $\overline{\lambda}_{p,mod}$ in a consistent manner, indicating that mathematical expression of the relationship can be used for predicting the structural resistance. It can also be observed that Eq. (2) based on original specifications in Eurocode 3 agrees well with the variation of $P_{u,plate}/A \times f_{2,\theta}$ with $\overline{\lambda}_{p,mod}$ for RHS stub columns. For the SHS stub columns, the $P_{u,plate}/A \times f_{2,\theta}$ for a specific $\overline{\lambda}_{p,mod}$ is relatively lower than that for RHS stub columns since the plates with lower widths in RHS can provide better restraints to the plate elements undergoing local buckling. To accurately estimate the resistance for SHS stub columns based on $\overline{\lambda}_{p,mod}$, Eq. (15) was generated to fit the variation of $P_{u,plate}/A \times f_{2,\theta}$ with $\overline{\lambda}_{p,mod}$ and to provide the lower bound based on the data obtained in this study. The accuracy of strength predictions ($P_{u,modEC3}$) based on the proposed modifications was evaluated statistically, as shown in Tables 2 and 3. The mean $P_{u,FE+Exp}/P_{u,modEC3}$ ratios are about 1.01–1.05 with CoV of 0.03–0.07. Compared with the $P_{u,EC3}$ obtained based on the original specifications in Eurocode 3, the modified approach provides more accurate and less scattered strength estimations, as shown in Tables 2 and 3.

$$\varepsilon_{\theta,mod} = \sqrt{\frac{235}{f_y}} \times \sqrt{\frac{k_{E,\theta}}{k_{y,\theta}}} \tag{14}$$

$$b_{e,mod} = b \times \frac{\overline{\lambda}_{p,mod}{}^{0.8} - 0.081 \times (3+\psi)}{\overline{\lambda}_{p,mod}{}^{2}} \quad for\ \overline{\lambda}_{p,mod} > 0.51 \tag{15}$$

4.2.1.2. Modification to AISC 360. The specifications given in AISC 360 for estimating the $P_{u,AISC}$ for stub columns with slender cross-sections are based on the λ_r, as shown in Eqs. (11)–(13). Thus, the estimation

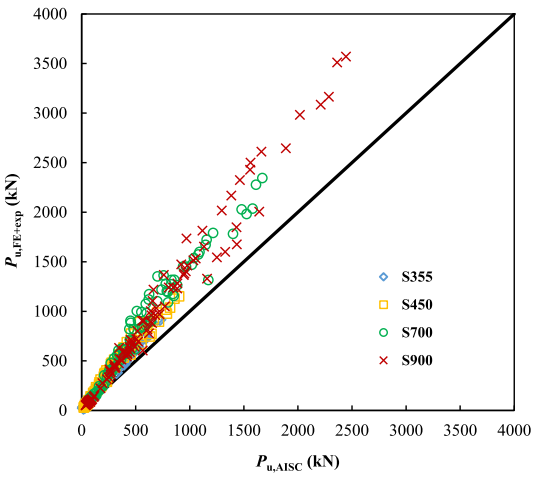

(a) SHS long columns

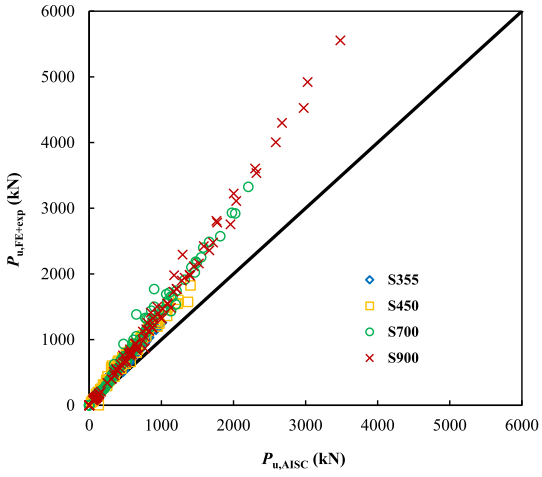

(b) RHS long columns buckling about major axis

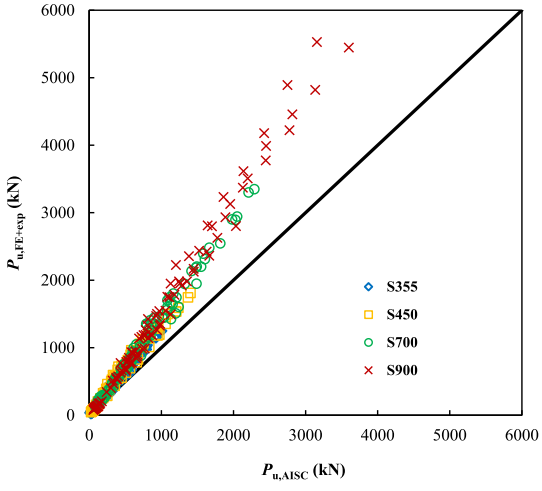

(c) RHS long columns buckling about minor axis

Fig. 10. Comparison of the strength predictions based on AISC 360 for cold-formed SHS and RHS long columns with those from parametric studies and experimental results in literature [20,21].

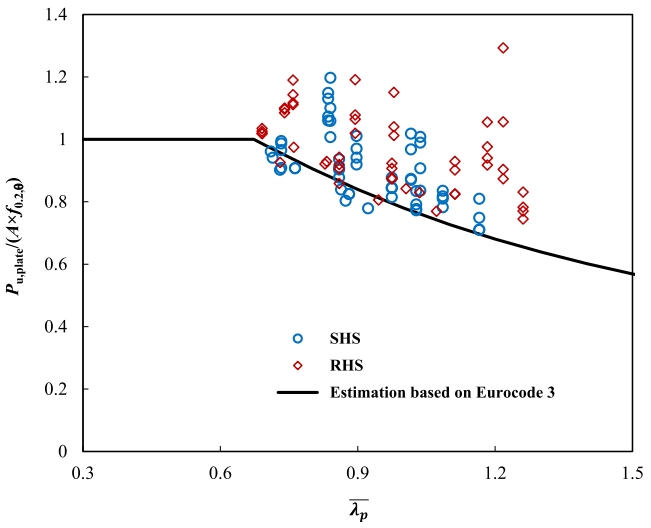

(a)

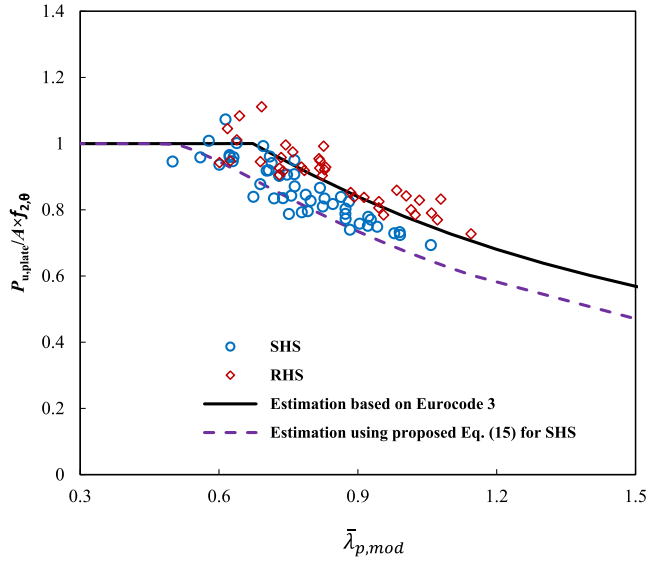

(b)

Fig. 11. Variation of normalised strength contribution ($P_{u,plate}$) from plate elements with non-dimensional slenderness of plates (a) based on original specifications in Eurocode 3 and (b) based on proposed modifications.

of λ_r can directly influence the accuracy of strength predictions. To obtain accurate estimation of λ_r for elevated temperature conditions, the $P_{u,plate}$ for plate elements of SHS and RHS stub columns were obtained and the normalised $P_{u,plate}$ by $A \times f_{2,\theta}$ are plotted against $\lambda/(\sqrt{\frac{E_\theta}{f_{2,\theta}}})$ in Fig. 12. The $f_{2,\theta}$ was adopted since the use of $f_{0.2,\theta}$ for strength predictions can lead to more significant underestimations of the resistance for the stub columns with non-slender cross-sections. As can be seen in Fig. 12, the λ_r as $1.4 \times \sqrt{\frac{E_\theta}{f_{2,\theta}}}$ is unsafe for those SHS and RHS stub columns under elevated temperatures and $\lambda_{r,mod}$ as $1.15 \times \sqrt{\frac{E_\theta}{f_{2,\theta}}}$ is proposed.

In order to develop an approach for safe and more accurate strength predictions, the variation of $P_{u,plate}/A \times f_{2,\theta}$ with $\lambda/\lambda_{r,mod}$ was obtained, as presented in Fig. 13. Based on the relationship in Fig. 13, Eq. (16) was generated through regression analysis by satisfying that *be* starts to reduce when λ reaches $\lambda_{r,mod}$, and the relationship from Eq. (16) agrees with the data for SHS and RHS stub columns with different grades as the lower bound. The $P_{u,modAISC}$ estimated based on the modified approach for SHS and RHS stub columns with slender cross-sections are compared with the $P_{u,FE+exp}$, as shown in Tables 2 and 3. The mean $P_{u,FE+exp}/P_{u,modAISC}$ ratio is about 1.01–1.06 with CoV of 0.02–0.06. Therefore, the modified approach can be applied to generate

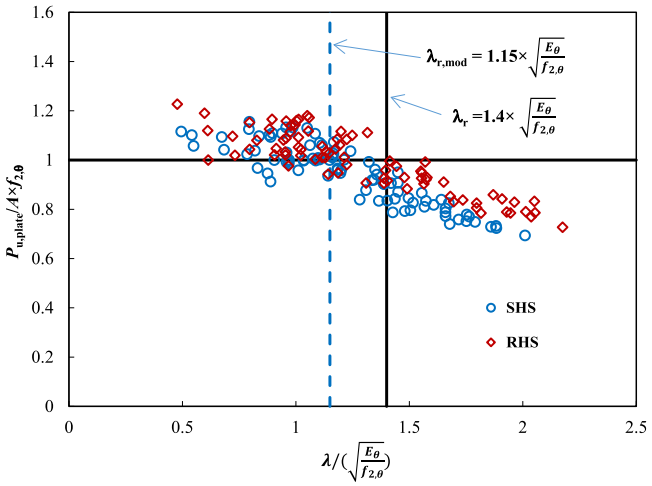

Fig. 12. The variation of normalised $P_{u,plate}$ with $\lambda/(\sqrt{\frac{E_\theta}{f_{2,\theta}}})$.

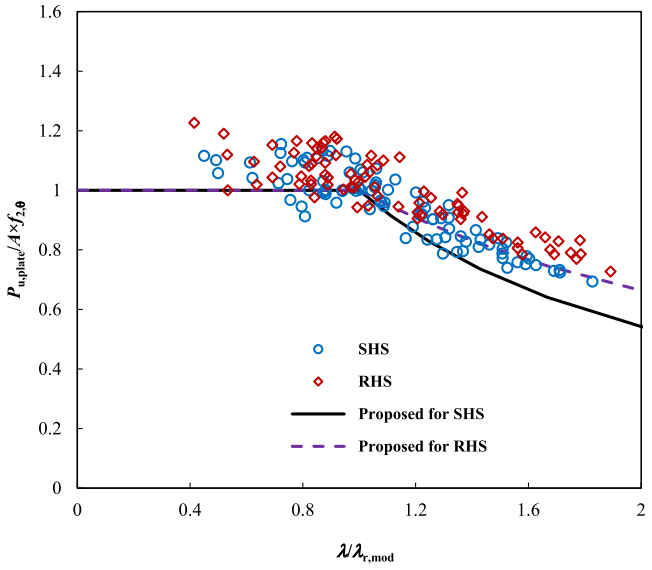

Fig. 13. Variation of normalised strength contribution ($P_{u,plate}$) with $\lambda/\lambda_{r,mod}$ ratios for plate elements of SHS and RHS columns.

more accurate and safe estimations of the resistance for SHS and RHS stub columns with slender cross-sections at elevated temperatures in comparison with those obtained based on the original approach in AISC 360.

$$b_e = \begin{cases} b\times\left[1.17\dfrac{\lambda_{r,mod}}{\lambda} - 0.17\times\left(\dfrac{\lambda_{r,mod}}{\lambda}\right)^2\right], \ for\ SHS \\ b\times\left[1.2\left(\dfrac{\lambda_{r,mod}}{\lambda}\right)^{0.75} - 0.2\times\left(\dfrac{\lambda_{r,mod}}{\lambda}\right)^2\right], \ for\ RHS \end{cases} \quad (16)$$

4.2.2. Design approaches for long columns

The strength predictions obtained based on existing design approaches in Eurocode 3 and AISC 360 for long columns were found to be significantly conservative, as discussed in Section 4.1. To reduce the conservativism for economical designs, more accurate approaches are needed for estimating the strengths of long SHS and RHS columns subject to elevated temperatures. Modifications to the approaches in Eurocode 3 and AISC 360 are proposed in the subsequent sections.

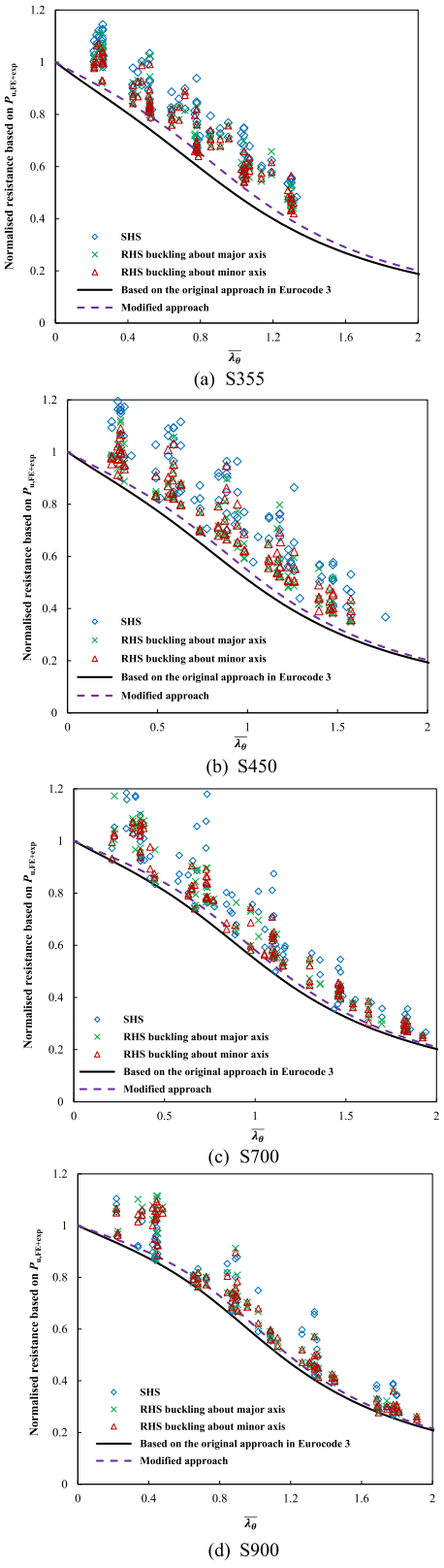

Fig. 14. Proposed χ_{EC} versus $\overline{\lambda_\theta}$ relationship based on the normalised resistance of SHS and RHS long columns.

4.2.2.1. Modification to Eurocode 3. The estimation of $P_{u,EC3}$ for long SHS and RHS columns at elevated temperatures is based on the estimation of cross-sectional resistance and the χ_{EC} versus $\overline{\lambda_\theta}$ relationship

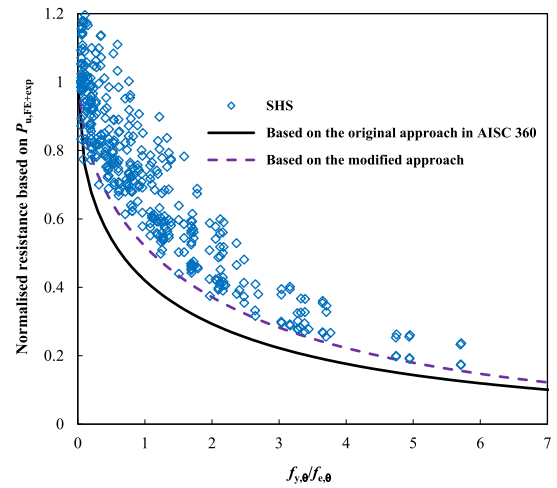

(a) SHS long columns

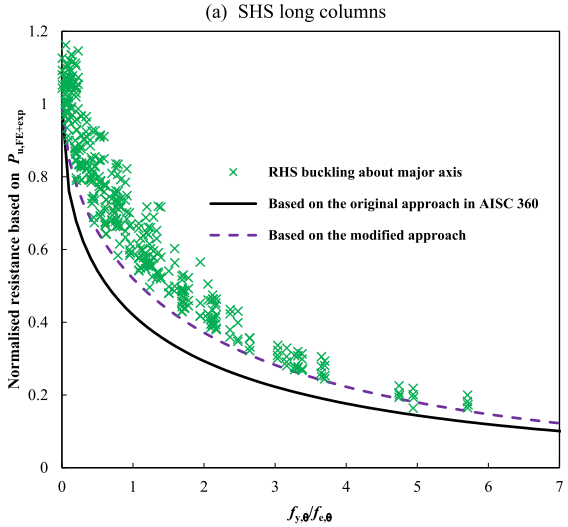

(b) RHS long columns buckling about major axis

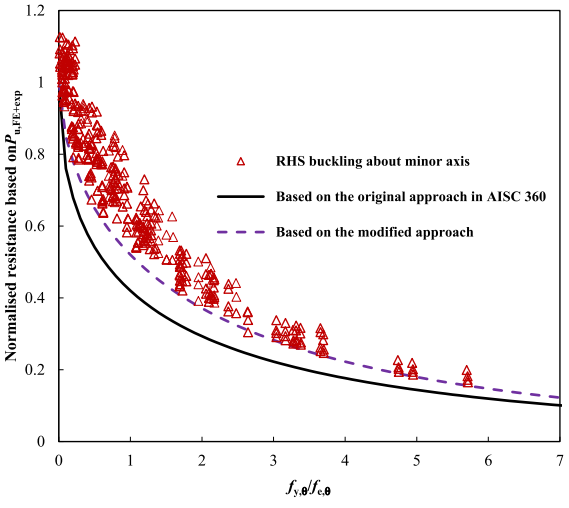

(c) RHS long columns buckling about minor axis

Fig. 15. Variation of normalised $P_{u,FE+exp}$ with $f_{y,\theta}/f_{e,\theta}$.

which is dependent on the parameter α. In addition to the proposed approaches in Section 4.2.1.1 for cross-sectional resistance predictions, to further improve the accuracy of predicting the resistance of the long columns, the $P_{u,FE+exp}$ for the structures are normalised by the cross-sectional resistance obtained based on Eurocode 3 for non-slender sections and the modified approach in Section 4.2.1.1 for slender sections, and subsequently plotted against $\overline{\lambda_\theta}$, as shown in Fig. 14. The relationship of χ_{EC} versus $\overline{\lambda_\theta}$ based on the α given as Eq. (6) is also shown in the figure. It can be seen in the figure that the χ_{EC} versus $\overline{\lambda_\theta}$ curve locates below the normalised $P_{u,FE+exp}$ data since the α was obtained by fitting limited data [30] without covering a wide range of steel grades. Based on the normalised $P_{u,FE+exp}$ versus $\overline{\lambda_\theta}$ obtained for the columns with different grades, a formula for calculating α_{mod} was generated, as given as Eq. (17). The statistical evaluation of the modified approach for long columns is presented in Table 4. The $P_{u,modEC3}$ values are 9%–33% on average lower than $P_{u,FE+exp}$ with CoV of 0.07–0.14. Compared with the $P_{u,EC3}$ obtained based on the original specifications in Eurocode 3, the modified approach generates more accurate and safe strength predictions, as shown in Table 4.

$$\alpha_{mod} = 0.52 \times \sqrt{235/f_y} \tag{17}$$

4.2.2.2. Modification to AISC 360. The $P_{u,AISC}$ predictions for the long columns were primarily based on the $F_{cr,\theta}$ in Eqs. (9) and (10). To improve the accuracy of strength predictions, a more accurate approach for estimating $F_{cr,\theta}$ would be required. Thus, the $P_{u,FE+exp}$ for the SHS and RHS long columns were normalised by the cross-sectional resistance obtained based on the original AISC 360 for those with non-slender sections and the modified approach in Section 4.2.1.2 for those with slender sections and the normalised $P_{u,FE+exp}$ are plotted against $f_{y,\theta}/f_{e,\theta}$, as shown in Fig. 15. As can be seen in the figures, the $F_{cr,\theta}$ calculated from Eq. (10) would lead to quite conservative strength predictions. Thus, Eq. (18) obtained through regression analysis is proposed to generate the $F_{cr,\theta}$ that agree better with the data for the columns, as demonstrated in Fig. 14. By using Eq. (18), more accurate $P_{u,modAISC}$ were obtained, as shown in Table 4 for the statistical evaluation.

$$F_{cr,\theta} = \left[0.52^{\left(\frac{f_{y,\theta}}{f_{e,\theta}}\right)^{0.6}}\right] \times f_{y,\theta} \tag{18}$$

5. Conclusions

The structural performance of cold-formed normal- and high-strength steel SHS and RHS columns at elevated temperatures was investigated through finite element modelling. A finite element model was developed with the validated capability of replicating the experimental results for the behaviour of those columns at ambient and elevated temperatures. Parametric studies were subsequently conducted on the cold-formed normal- and high-strength steel SHS and RHS stub and long columns with a wide range of cross-sectional dimensions, member slenderness and steel grades and subject to various elevated temperatures up to 800 °C. The ultimate loads obtained for the stub and long columns through parametric studies and those from experimental investigations in literature were compared with the column strengths predicted based on specifications in Eurocode 3 and AISC 360 standards. The comparison shows that the Eurocode 3 underestimates the strengths for the stub and long columns at elevated temperatures for up to 40% on average. As for the AISC 360 standard, unconservative strength predictions were obtained primarily for the SHS stub columns and S355 and S450 RHS stub columns while the standard generates quite conservative predictions for the ultimate loads of SHS and RHS long columns. To improve the accuracy of strength predictions, modifications to the design approaches in the standards were proposed. The modified approaches provide more accurate strength predictions than those based on original design approaches in the standards and thus are recommended to be used for the design of the cold-formed normal- and high-strength steel SHS and RHS columns under elevated temperatures.

CRediT authorship contribution statement

Han Fang: Writing – original draft, Project administration, Methodology, Investigation, Conceptualization. **Tak-Ming Chan:** Writing – review & editing.

Declaration of competing interest

The authors declare that they have no known competing financial interests or personal relationships that could have appeared to influence the work reported in this paper.

Data availability

Data will be made available on request.

References

[1] J. Wardenier, J.A. Packer, X.L. Zhao, G.J. van der Vegte, Hollow Sections in Structural Applications, second ed., CIDECT, Geneva, 2010.

[2] B. Cheng, Q. Qian, X.L. Zhao, Tests to determine stress concentration factors for square bird-beak SHS joints under chord and brace axial forces, J. Struct. Eng. 140 (11) (2014) 04014088.

[3] H.X. Liu, H. Fang, J.Y. Zhu, T.M. Chan, Numerical investigation on the structural performance of octagonal hollow section columns, Structures 34 (2021) 3257–3267.

[4] X. Meng, L. Gardner, Cross-sectional behaviour of cold-formed high strength steel circular hollow sections, Thin-Walled Struct. 156 (2020a) 106822.

[5] O. Skoglund, J. Leander, R. Karouml, Overview of steel bridges containing high strength steel, Int. J. Steel Struct. 20 (4) (2020) 1294–1301.

[6] K. Ke, M.C.H. Yam, H.Y. Zhang, A.C.C. Lam, X.H. Zhou, High-strength steel frames with SMA connections in self-centring energy-dissipation bays: insights and a multimodal nonlinear static procedure, Smart Mater. Struct. 29 (2020) 125020.

[7] M.C.H. Yam, K. Ke, B.H. Jiang, A.C.C. Lam, Net section resistance of bolted S690 steel angles subjected to tension, Thin-Walled Struct. 151 (2020) 106722.

[8] H. Fang, T.M. Chan, B. Young, Structural performance of cold-formed high strength steel tubular columns, Eng. Struct. 177 (2018) 473–488.

[9] J.B. Chen, H. Fang, T.M. Chan, Design of fixed-ended octagonal shaped steel hollow sections in compression, Eng. Struct. 228 (2021) 111520.

[10] J.L. Ma, T.M. Chan, B. Young, Experimental investigation on stub-column behavior of cold-formed high strength steel tubular sections, J. Struct. Eng. 142 (5) (2016) 04015174.

[11] J.L. Ma, T.M. Chan, B. Young, Design of cold-formed high strength steel tubular beams, Eng. Struct. 151 (2017) 432–443.

[12] J.L. Ma, T.M. Chan, B. Young, Cold-formed high-strength steel rectangular and square hollow sections under combined compression and bending, J. Struct. Eng. 145 (12) (2019) 04019154.

[13] H. Fang, T.M. Chan, B. Young, Experimental and numerical investigations of octagonal high-strength steel tubular stub columns under combined compression and bending, J. Struct. Eng. 147 (1) (2021) 04020282.

[14] X. Meng, L. Gardner, Stability and design of normal and high strength steel CHS beam–columns, Eng. Struct. 251 (2022) 113361.

[15] W. Chen, J.H. Ye, Y. Bai, X.L. Zhao, Full-scale fire experiments on load-bearing cold-formed steel walls lined with different panels, J. Construct. Steel Res. 79 (2012) 242–252.

[16] M.T. Chen, M. Pandey, B. Young, Mechanical properties of cold-formed steel semi-oval hollow sections after exposure to ISO-834 fire, Thin-Walled Struct. 167 (2021) 108202.

[17] H. Fang, B. Wong, Y. Bai, Kinetic modelling of thermophysical properties of shape memory alloys during phase transformation, Constr. Build. Mater. 131 (2017) 146–155.

[18] H.T. Li, B. Young, Material properties of cold-formed high strength steel at elevated temperatures, Thin-Walled Struct. 115 (2017) 289–299.

[19] L. Gardner, N. Saari, F. Wang, Comparative experimental study of hot-rolled and cold-formed rectangular hollow sections, Thin-Walled Struct. 48 (2010) 495–507.

[20] J.L. Ma, Behaviour and Design of Cold-Formed High Strength Steel Tubular Members, (Ph.D. thesis), Department of Civil Engineering, The University of Hong Kong, 2016.

[21] M. Balarupan, M. Mahendran, Experimental studies of cold-formed steel hollow section columns at elevated temperatures, in: Proceedings of the Annual Stability Conference Structural Stability Research Council, Toronto, Canada, 2014.

[22] H. Fang, T.M. Chan, Resistance of axially loaded hot-finished S460 and S690 steel square hollow stub columns at elevated temperatures, Structures 17 (2019a) 66–73.

[23] M. Kucukler, Compressive resistance of high-strength and normal-strength steel CHS members at elevated temperatures, Thin-Walled Struct. 152 (10753) (2020).

[24] A. Mohammed, K.A. Cashell, Structural fire design of SHS, RHS and CHS high strength steel columns, Adv. Struct. Eng. (2021) 13694332211001498.

[25] W.M. Quach, B. Young, Material properties of cold-formed and hot-finished elliptical hollow sections, Adv. Struct. Eng. 18 (2015) 1101–1114.

[26] M. Feng, Y.C. Wang, J.M. Davies, A numerical imperfection sensitivity study of cold-formed thin-walled tubular steel columns at uniform elevated temperatures, Thin-Walled Struct. 42 (2004) 533–555.

[27] EN 1993-1-2, Eurocode 3: Design of Steel Structures-Part 1-2: General Rules-Structural Fire Design, European Committee for Standardization, Brussels, 2005.

[28] ANSI/AISC 360-16, Specification for Structural Steel Buildings, AISC, Chicago, 2016.

[29] ABAQUS [Computer Software] Version 6.14, Dassault Systèmes, Providence, RI, 2012.

[30] H. Fang, T.M. Chan, Axial compressive strength of welded S460 steel columns at elevated temperatures, Thin-Walled Struct. 129 (2018) 213–224.

[31] Y. Huang, J. Chen, Y. He, B. Young, Design of cold-formed stainless steel RHS and SHS beam–columns at elevated temperatures, Thin-Walled Struct. 165 (2021) 107960.

[32] E. Steau, M. Mahendran, Thermal modelling of LSF floor-ceiling systems with varying configurations, Fire Saf. J. 118 (2020) 103227.

[33] Y.C. Cai, F. Zhou, L.P. Wang, B. Young, Design of lean duplex stainless steel tubular sections subjected to concentrated end bearing loads at elevated temperatures, Thin-Walled Struct. 160 (2021a) 107298.

[34] Y.C. Cai, T.M. Chan, B. Young, Chord plastification in high strength steel circular hollow section X-joints: Testing, modelling and strength predictions, Eng. Struct. 243 (2021b) 112692.

[35] H. Fang, P. Visintin, Structural performance of geopolymer-concrete-filled steel tube members subjected to compression and bending, J. Construct. Steel Res. 188 (2022) 107026.

[36] M. Balarupan, Structural Behaviour and Design of Cold-Formed Steel Hollow Section Columns under Simulated Fire Condition, (Ph.D. thesis), School of Civil Engineering and Built Environmet, Queensland University of Technology, 2015.

[37] L. Gardner, X. Yun, Description of stress–strain curves for cold-formed steels, Constr. Build. Mater. 189 (2018) 527–538.

[38] H. Fang, T.M. Chan, Buckling resistance of welded high-strength-steel box-section members under combined compression and bending, J. Construct. Steel Res. 162 (2019b) 105711.

[39] K.R. Rasmussen, G.J. Hancock, Design of cold-formed stainless steel tubular members. I: columns, J. Struct. Eng. 119 (1993) 2349–2367.

[40] J.Z. Liu, H. Fang, T.M. Chan, Investigations on material properties and residual stresses in cold-formed high strength steel irregular hexagonal hollow sections, Thin-Walled Struct. 176 (2022) 109220.

[41] J.L. Ma, T.M. Chan, B. Young, Material properties and residual stresses of cold-formed high strength steel hollow sections, J. Construct. Steel Res. 109 (2015) 152–165.

[42] M. Imran, M. Mahendran, P. Keerthan, Mechanical properties of cold-formed steel tubular sections at elevated temperatures, J. Construct. Steel Res. 143 (2018) 131–147.

[43] H.T. Li, B. Young, Cold-formed high strength steel SHS and RHS beams at elevated temperatures, J. Construct. Steel Res. 158 (2019) 475–485.

[44] X. Meng, L. Gardner, Behavior and design of normal- and high-strength steel SHS and RHS columns, J. Struct. Eng. 146 (11) (2020b) 04020227.

[45] EN 1993-1-5, Eurocode 3: Design of Steel Structures - Part 1-5: Plated Structural Elements, CEN, Brussels, Belgium, 2006.

[46] C. Couto, P.V. Real, N. Lopes, B. Zhao, Effective width method to account for the local buckling of steel thin plates at elevated temperatures, Thin-Walled Struct. 84 (2014) 134–149.

[47] C. Couto, T. Coderre, P.V. Real, N. Boissonnade, Cross-section capacity of RHS and SHS at elevated temperatures: Comparison of design methodologies, Structures 34 (2021) 198–214.